Journal of Fluids and Structures (2000) **14,** 895–916
doi:10.1006/jfls.2000.0301, available online at http://www.idealibrary.com on IDEAL®

DIVERGENCE INSTABILITY OF VARIABLE-ARC-LENGTH ELASTICA PIPES TRANSPORTING FLUID

S. CHUCHEEPSAKUL AND T. MONPRAPUSSORN

Department of Civil Engineering, King Mongkut's University of Technology Thonburi Bangkok 10140, Thailand

(Received 28 June 1999, and in final form 5 April 2000)

A flexible elastic pipe transporting fluid is held by an elastic rotational spring at one end, while at the other end, a portion of the pipe may slide on a frictional support. Regardless of the gravity loads, when the internal flow velocity is higher than the critical velocity, large displacements of static equilibrium and divergence instability can be induced. This problem is highly nonlinear. Based on the inextensible elastica theory, it is solved herein via the use of elliptic integrals and the shooting method. Unlike buckling with stable branching of a simply supported elastica pipe with constant length, the variable arc-length elastica pipe buckles with unstable branching. The friction at the support has an influence in shifting the critical locus over the branching point. Alteration of the flow history causes jumping between equilibrium paths due to abrupt changes of direction of the support friction. The elastic rotational restraint brings about unsymmetrical bending configurations; consequently, snap-throughs and snap-backs can occur on odd and even buckling modes, respectively. From the theoretical point of view, the equilibrium configurations could be formed like soliton loops due to snapping instability.
© 2000 Academic Press

1. INTRODUCTION

A CONSIDERABLE AMOUNT OF RESEARCH WORK was done concerning the problems of a pipe conveying fluid as mentioned in the papers by Chen (1974), Païdoussis and Issid (1974), and in the textbooks by Thompson (1982), Blevins (1990), and more recently by Païdoussis (1998). Most of researchers determined stability criteria based on the small displacement theory. This conventional approach, however, does not take into consideration the post-buckling information, which supplements the lucid understanding of the mechanisms of large deflection of pipes transporting fluid, and are indispensable to the design of nonlinear system operation control. After publication of the paper by Thompson & Lunn (1981), the static elastica theory is an alternative approach for nonlinear analysis of pipes conveying fluid in the case where the pipe is dominated by divergence instability. In that study, the elastica pipe was considered to have a constant arc-length.

Nevertheless, in some applications, the arc-length of pipe is not constant and it could vary during operations. One may call such a pipe a variable-arc-length (VAL) pipe. Marine risers employed in deep-ocean mining (Huang & Chucheepsakul 1985) are examples of the variable-arc-length pipe. The riser is a flexible conductor pipe, which extends from the ball joint of the wellhead at seabed to the slip joint beneath the vessel. The slip joint allows the riser to change its length as the vessel heaves and moves laterally; consequently, the longitudinal strain is small and the effects of extensibility are negligible. Because of large deflection behaviour under offshore environment, the initial (equilibrium)

0889–9746/00/080895 + 22 $35.00/0 © 2000 Academic Press

configuration of the riser may be defined as a VAL elastica and the riser behaves as a VAL elastica pipe.

To the authors' knowledge, the problem of VAL elastica pipes transporting fluid has not yet been considered in the past, thus it is the purpose of this study to explore the post-buckling behaviour and to investigate the possible equilibrium configurations of VAL elastica pipes transporting fluid. Figure 1(a) illustrates the VAL pipe studied herein. The pipe is installed on two stationary supports with a span length L and an overhang length ℓ. One end is held by the pinned support A of elastic rotational spring constant K, whereas the other end-portion is propped by the support B with a static friction coefficient μ. After buckling, it can slide over support B.

The literature review on various cases of the VAL pipe may be summarized as follows.

(i) For $K = 0$ and $\ell/L = 0$ the VAL pipe becomes a simply supported pipe, which cannot flutter, as reported by Holmes (1978).

(ii) For $K = 0$ and $\ell/L = 0{\cdot}582$ the VAL pipe is an overhung pipe. Following the equivalent force analogy given by Thompson & Lunn (1981), the results of Elishakoff & Lottati (1988) show that if $\ell/L < 0{\cdot}582$ the pipe is dominated by divergence, if $\ell/L > 0{\cdot}582$ the pipe is dominated by flutter, and if $\ell/L = 0{\cdot}582$ the pipe is in transition between divergence and flutter instability.

(iii) For $K = \infty$ and $\ell/L = 0$ the VAL pipe is a propped cantilever pipe. The experimental and theoretical results given by Yoshizawa *et al.* (1985) show that the pipe does lose stability by divergence.

(iv) For $K = \infty$ and $\ell/L \approx 0{\cdot}686$. The experimental results given by Jendrzejczyk & Chen (1983) show that if $\ell/L < 0{\cdot}686$ the pipe is dominated by divergence, if $\ell/L > 0{\cdot}686$ the pipe is dominated by flutter, and if $\ell/L = 0{\cdot}686$ the pipe is at a transition point between divergence and flutter instability. The finite element solutions excluding the effects of gravity forces and fluid pressures given by Escobar & Ting (1986) arrived at the same deduction, but for the transition condition $\ell/L = 0{\cdot}643$.

(v) For $K = \infty$ and $\ell/L = \infty$ the VAL pipe becomes a cantilevered pipe, which behaves as Beck's problem (Beck 1952) and thus flutter instability dominates, as shown by Gregory & Païdoussis (1966).

It is inferred from the above review that the condition that the VAL pipe could be dominated by divergence is $\ell/L < 0{\cdot}582$–$0{\cdot}686$ for $K = 0$ to ∞. From a practical point of view, this condition is sufficient but not necessary; it is speculated that the VAL pipe with any value of ℓ/L behaves as an elastica pipe if the transported fluid is suddenly jetted over the divergence velocity by a high-pressure pump. This situation, that the divergence instability always dominates, is used as the main assumption of this study.

The static elastica formulation can be achieved by consideration of equilibrium conditions between interacting fluid and pipe elements. The governing nonlinear differential equation obtained for elasticas, together with the boundary conditions, is solved analytically using elliptic integrals. As an independent check, the shooting method is also used to obtain numerical solutions. The effects of spring stiffness and friction at the supports on the stability criteria and post-buckling behaviour are studied and described in detail. Extensive bending results are presented graphically and snap-bending incidents are highlighted.

2. ELASTICA FORMULATION

Figure 1(b) shows diagrams of the interacting fluid and pipe infinitesimal elements. The transported fluid element is of density ρ_i, steady flow speed U, pressure p_i, and frictional drag force τ, whereas an infinitesimal arc-length ds of the elastica pipe is of inner

cross-sectional area A_i and flexural rigidity EI. The positive directions of bending moment M, vertical and normal shear forces V and Q, and horizontal and tangential forces H and T, in the intrinsic coordinate (s, θ), are assigned in accordance with bending of a radius of gyration r and positive curvature κ as shown in Figure 1(b). Elastic buckling occurs after the critical flow velocity as shown in Figure 1(c). It should be noted that despite sliding of the pipe end-portion, the pipe tip E is assumed not to fall off the support B in the mathematical treatment herein, because such a case is irrelevant to the VAL elastica pipe.

Figure 1(d) shows a free-body diagram of forces acting on an elastica pipe segment. When the equilibrium of forces in the $\hat{n}$ and $\hat{t}$ directions of the diagrams of Figure 1(b) are considered, and the equilibrium of moments is taken about the centre point O of the pipe element (the derivation is given in Appendix A), the internal force equations are obtained as

$$\frac{\mathrm{d}N}{\mathrm{d}\theta} - Q = 0, \quad \frac{\mathrm{d}Q}{\mathrm{d}\theta} + N = 0, \quad \frac{\mathrm{d}M}{\mathrm{d}s} - Q = 0, \tag{1a–c}$$

where $N = T - p_i A_i - \rho_i A_i U^2$ is the combined tension (Moe & Chucheepsakul 1988). Based on the constitutive equation of elastica theory,

$$M = -EI\frac{\mathrm{d}\theta}{\mathrm{d}s} \tag{2}$$

with some manipulation of equation (1), the second-order differential equations are

$$\frac{\mathrm{d}^2N}{\mathrm{d}\theta^2} + N = 0, \quad \frac{\mathrm{d}^2Q}{\mathrm{d}\theta^2} + Q = 0, \quad EI\frac{\mathrm{d}^2\theta}{\mathrm{d}s^2} + Q = 0. \tag{3a–c}$$

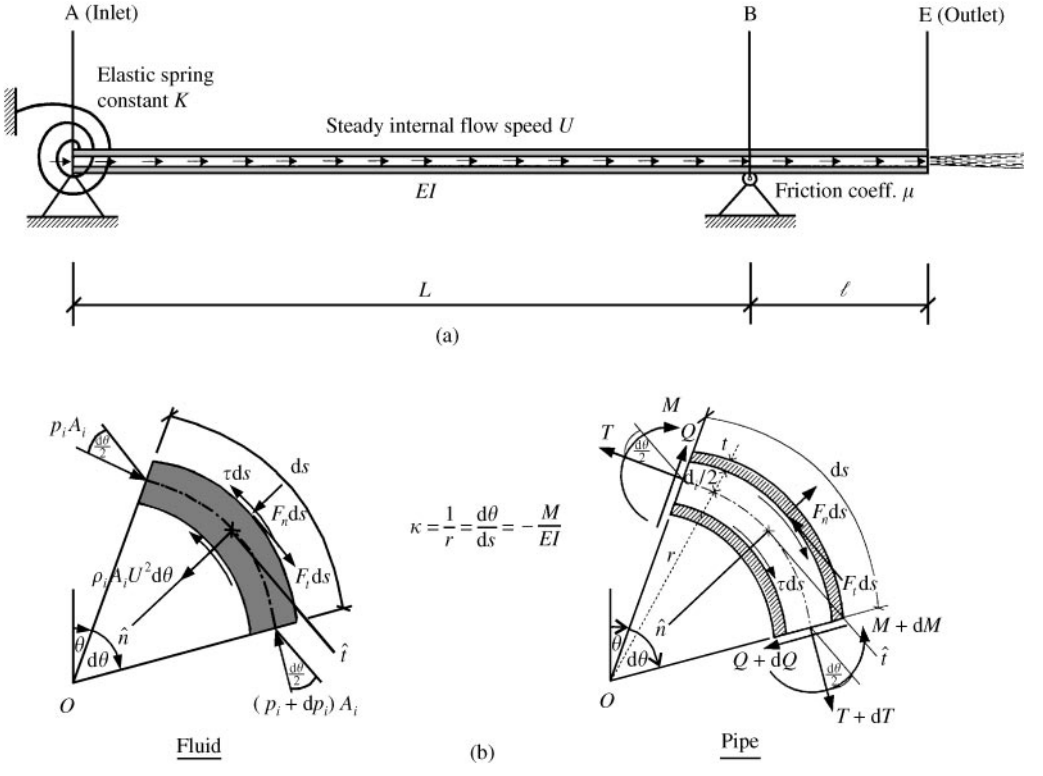

Figure 1. The variable-arc-length (VAL) elastica pipe transporting fluid: (a) undeformed configuration; (b) interaction diagrams of an elastica segment.

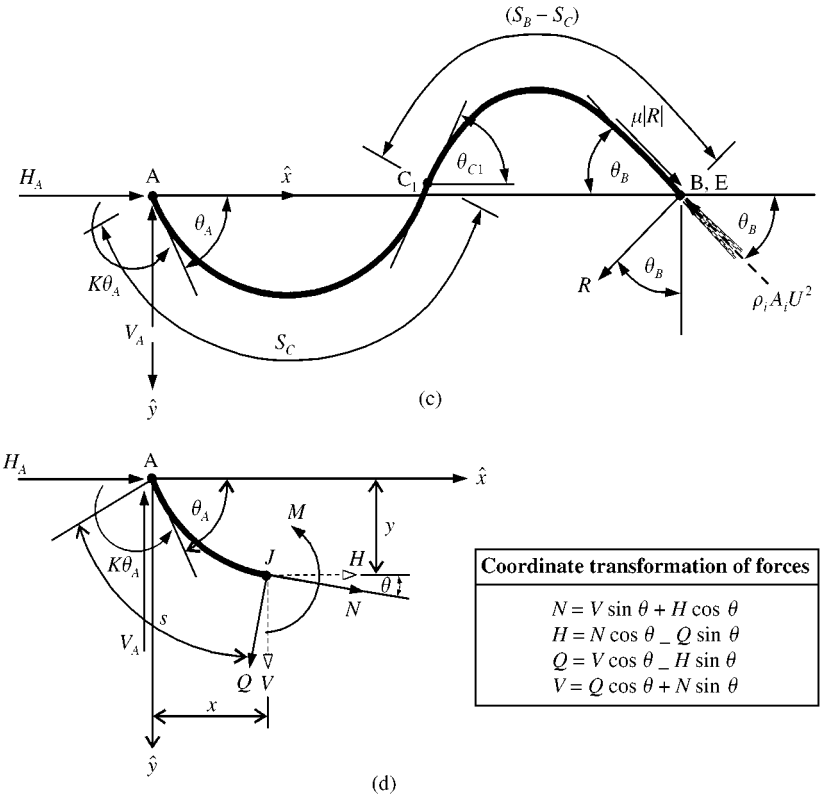

Figure 1. (continued) (c) a post-buckling configuration;(d) a free-body diagram of an elastica segment.

The general solution of equations (3) together with geometric relations and transformation of forces as shown in Figure 1(d) yield the set of equations describing plane deformations of elasticas transporting fluid, namely

$$N = -C_1 \cos\theta + C_2 \sin\theta, \quad H = -C_1, \quad \frac{dx}{ds} = \cos\theta,$$

$$Q = C_1 \sin\theta + C_2 \cos\theta, \quad V = C_2, \quad \frac{dy}{ds} = \sin\theta, \tag{4a–h}$$

$$M = C_1 y + C_2 x + C_3, \quad EI\frac{d^2\theta}{ds^2} + C_1 \sin\theta + C_2 \cos\theta = 0,$$

where C_1, C_2 and C_3 are arbitrary constants.

The boundary conditions (BCs) of the VAL elastica shown in Figure 1(c) are as follows:

Geometric BCs	*Natural BCs*	
Support A: $(x, y) = (0, 0)$, $(s, \theta) = (0, \theta_A)$,	$M = -K\theta_A$;	(5a–c)
Support B: $(x, y) = (L, 0)$, $(s, \theta) = (s_B, \theta_B)$,	$M = 0$, $Q = R$, $T = \mu\|R\|$;	(5d–h)
Outlet end E: $p_i = 0$,	$N = \mu\|R\| - \rho_i A_i U^2$.	(5i, j)

Once the boundary conditions (5) are applied to equations (4), the constants C_1–C_3 and the support reaction R are determined and written as

$$C_1 = \rho_i A_i U^2(\cos\theta_B + \Lambda \sin\theta_B) + \Lambda \frac{K\theta_A}{L}, \quad C_2 = \frac{K\theta_A}{L}, \quad C_3 = -K\theta_A,$$
$$R = \frac{\rho_i A_i U^2 L \sin\theta_B + K\theta_A}{L(\cos\theta_B \pm \mu \sin\theta_B)}, \quad \Lambda = \tan(\theta_B \mp \omega), \tag{6a–e}$$

where $\omega = \tan^{-1}\mu$ is the friction angle. The signs $\pm$ and $\mp$ in equations (6d,e) take care of the value of $|R|$. Substituting equations (6) into (4) yields the governing equations of this problem:

$$N = -\left[\rho_i A_i U^2(\cos\theta_B + \Lambda \sin\theta_B) + \frac{\Lambda K\theta_A}{L}\right]\cos\theta + \frac{K\theta_A}{L}\sin\theta,$$
$$H = -\rho_i A_i U^2(\cos\theta_B + \Lambda \sin\theta_B) + \frac{\Lambda K\theta_A}{L}; \quad \frac{\mathrm{d}x}{\mathrm{d}s} = \cos\theta,$$
$$Q = \left[\rho_i A_i U^2(\cos\theta_B + \Lambda \sin\theta_B) + \frac{\Lambda K\theta_A}{L}\right]\sin\theta + \frac{K\theta_A}{L}\cos\theta,$$
$$V = \frac{K\theta_A}{L}, \quad \frac{\mathrm{d}y}{\mathrm{d}s} = \sin\theta, \tag{7a–h}$$
$$M = \left[\rho_i A_i U^2(\cos\theta_B + \Lambda \sin\theta_B) + \frac{\Lambda K\theta_A}{L}\right]y + \frac{K\theta_A}{L}x - K\theta_A,$$
$$EI\frac{\mathrm{d}^2\theta}{\mathrm{d}s^2} + \left[\rho_i A_i U^2(\cos\theta_B + \Lambda \sin\theta_B) + \frac{\Lambda K\theta_A}{L}\right]\sin\theta + \frac{K\theta_A}{L}\cos\theta = 0.$$

Thompson & Lunn (1981) showed that equations (7) can also be obtained from analysis of the empty pipe subjected to the end follower force $\rho_i A_i U^2$ shown in Figure 1(c).

3. ELLIPTIC INTEGRAL SOLUTION

The following dimensionless quantities are introduced for the sake of generality:

$$\bar{x} = \frac{x}{L}, \quad \bar{y} = \frac{y}{L}, \quad \bar{s} = \frac{s}{L}, \quad s^* = \frac{s}{s_B}, \quad \bar{s}_B = \frac{s_B}{L}, \quad \bar{K} = \frac{KL}{EI}, \quad \bar{U} = \frac{\rho_i A_i U^2 L^2}{EI}, \tag{8a–g}$$

where s_B is the total arc-length of an elastica pipe. Then, equations (7h), (5c,f) and the n inflection conditions corresponding to the n unknowns $\theta_{c1}, \theta_{c2}, \ldots, \theta_{cn}$ (which are used in the integration to determine the elastica solutions), can be written in a nondimensional form

$$\frac{\mathrm{d}^2\theta}{\mathrm{d}\bar{s}^2} + [\bar{U}(\cos\theta_B + \Lambda \sin\theta_B) + \Lambda\bar{K}\theta_A]\sin\theta + \bar{K}\theta_A\cos\theta = 0, \tag{9a}$$

$$\left.\frac{\mathrm{d}\theta}{\mathrm{d}\bar{s}}\right|_{\theta=\theta_A} = \bar{K}\theta_A, \quad \left.\frac{\mathrm{d}\theta}{\mathrm{d}\bar{s}}\right|_{\theta=\theta_B} = 0, \tag{9b,c}$$

$$\left.\frac{\mathrm{d}\theta}{\mathrm{d}\bar{s}}\right|_{\theta=\theta_{c_1}} = \left.\frac{\mathrm{d}\theta}{\mathrm{d}\bar{s}}\right|_{\theta=\theta_{c_2}} = \cdots = \left.\frac{\mathrm{d}\theta}{\mathrm{d}\bar{s}}\right|_{\theta=\theta_{c_n}} = 0 \quad \text{in which } n = m + n_s - 1. \tag{9d}$$

Let m be the order of the buckling mode and n_s the number of rotational springs, here $n_s = 0$ for $K = 0$ and $n_s = 1$ for $K \neq 0$. The subscripts A, B, C_1, C_2, …, C_n denote quantities evaluated at the support points A, B and at the inflection points $C_1, C_2, \ldots, C_n$, respectively.

Upon integrating equation (9a) with respect to θ and applying equations (9b–d), the following set of first-order differential equations and the $n + 1$ constraint equations are obtained:

$$\bar{\kappa} = \frac{\mathrm{d}\theta}{\mathrm{d}\bar{s}} = \pm\sqrt{a + b\sin\theta + c\cos\theta}, \quad \frac{\mathrm{d}\bar{x}}{\mathrm{d}\bar{s}} = \cos\theta, \quad \frac{\mathrm{d}\bar{y}}{\mathrm{d}\bar{s}} = \sin\theta, \tag{10a–c}$$

$$\begin{aligned}
&b(\sin\theta_B - \sin\theta_A) + c(\cos\theta_B - \cos\theta_A) + \bar{K}^2\theta_A^2 = 0,\\
&b(\sin\theta_B - \sin\theta_{C_1}) + c(\cos\theta_B - \cos\theta_{C_1}) = 0,\\
&b(\sin\theta_B - \sin\theta_{C_2}) + c(\cos\theta_B - \cos\theta_{C_2}) = 0,\\
&\qquad\vdots \qquad\qquad\qquad \vdots \qquad\qquad \vdots\\
&b(\sin\theta_B - \sin\theta_{C_n}) + c(\cos\theta_B - \cos\theta_{C_n}) = 0,
\end{aligned} \tag{11}$$

where

$$a = -b\sin\theta_B - c\cos\theta_B, \quad b = -2\bar{K}\theta_A, \quad c = 2[\bar{U}(\cos\theta_B + \Lambda\sin\theta_B) + \Lambda\bar{K}\theta_A]. \tag{12a–c}$$

The minus sign ($-$) of the dimensionless curvature $\bar{\kappa}$ is for the concave curve, whereas the plus sign ($+$) is for the convex curve of elastica portions.

The integration and mapping of equations (10) by elliptic integrals (Byrd and Friedman 1971) yield the closed-form solutions of equilibrium configurations as follows in tabular form:

Coordinates refer from the point A to any Z	The interval containing a point Z is from				
	A to C_1	C_1 to C_2	⋯	C_n to B	
$\bar{s}_Z =$	$\bar{s}_{AZ}$	$\bar{s}_{AC_1} + \bar{s}_{C_1Z}$	⋯	$\bar{s}_{AC_1} + \bar{s}_{C_1C_2} + \cdots + \bar{s}_{C_{n-1}C_n} + \bar{s}_{C_nZ}$	(13)
$\bar{x}_Z =$	$\bar{x}_{AZ}$	$\bar{x}_{AC_1} + \bar{x}_{C_1Z}$	⋯	$\bar{x}_{AC_1} + \bar{x}_{C_1C_2} + \cdots + \bar{x}_{C_{n-1}C_n} + \bar{x}_{C_nZ}$	(14)
$\bar{y}_Z =$	$\bar{y}_{AZ}$	$\bar{y}_{AC_1} + \bar{y}_{C_1Z}$	⋯	$\bar{y}_{AC_1} + \bar{y}_{C_1C_2} + \cdots + \bar{y}_{C_{n-1}C_n} + \bar{y}_{C_nZ}$	(15)

In equations (13)–(15),

$$\bar{s}_{ij} = \int_{\theta_i}^{\theta_j} \frac{\mathrm{d}\theta}{\bar{\kappa}} = \begin{cases} \dfrac{\sqrt{2}}{(b^2 + c^2)^{1/4}}[\mathrm{F}(\Phi_j, k) - \mathrm{F}(\Phi_i, k)] & \text{for } \theta_j \geq \theta_i \text{ of positive } \bar{\kappa}, \\ \dfrac{\sqrt{2}}{(b^2 + c^2)^{1/4}}[\mathrm{F}(\Phi_i, k) - \mathrm{F}(\Phi_j, k)] & \text{for } \theta_j < \theta_i \text{ of negative } \bar{\kappa}, \end{cases} \tag{16}$$

$$\bar{x}_{ij} = \int_{\theta_i}^{\theta_j} \frac{\cos\theta\,\mathrm{d}\theta}{\bar{\kappa}} = \begin{cases} \dfrac{\sqrt{2}c}{(b^2 + c^2)^{3/4}}\left[\eta(\Phi_j, k) - \eta(\Phi_i, k) + \dfrac{2kb}{c}(\cos\Phi_j - \cos\Phi_i)\right] & \text{for } \theta_j \geq \theta_i, \\ \dfrac{\sqrt{2}c}{(b^2 + c^2)^{3/4}}\left[\eta(\Phi_i, k) - \eta(\Phi_j, k) + \dfrac{2kb}{c}(\cos\Phi_i - \cos\Phi_j)\right] & \text{for } \theta_j < \theta_i, \end{cases} \tag{17}$$

$$\bar{y}_{ij} = \int_{\theta_i}^{\theta_j} \frac{\sin\theta \, \mathrm{d}\theta}{\bar{\kappa}} = \begin{cases} \dfrac{\sqrt{2}b}{(b^2+c^2)^{3/4}}\left[\eta(\Phi_j, k) - \eta(\Phi_i, k) - \dfrac{2kc}{b}(\cos\Phi_j - \cos\Phi_i)\right] & \text{for } \theta_j \geq \theta_i, \\ \dfrac{\sqrt{2}b}{(b^2+c^2)^{3/4}}\left[\eta(\Phi_i, k) - \eta(\Phi_j, k) - \dfrac{2kc}{b}(\cos\Phi_i - \cos\Phi_j)\right] & \text{for } \theta_j < \theta_i, \end{cases} \tag{18}$$

in which the following parameters are prescribed in mapping:

$$\eta(\Phi_i, k) = 2\mathrm{E}(\Phi_i, k) - \mathrm{F}(\Phi_i, k), \quad \varphi = \sin^{-1}\left(\frac{b}{p}\right) = \cos^{-1}\left(\frac{c}{p}\right), \tag{19a–e}$$

$$\Phi_i = \sin^{-1}\left(\sqrt{\frac{p - b\sin\theta_i - c\cos\theta_i}{a+p}}\right), \quad k = \sqrt{\frac{a+p}{2p}}, \quad p = \sqrt{b^2+c^2}.$$

The functions $\mathrm{F}(\Phi, k)$ and $\mathrm{E}(\Phi, k)$ are the adjustable elliptic integrals of the first and second kind, respectively, defined as

$$\mathrm{F}(\Phi, k) = \mathrm{sgn}(\theta) \times \{\text{Jacobi's standard elliptic integrals of the first kind}\}, \tag{19f}$$

$$\mathrm{E}(\Phi, k) = \mathrm{sgn}(\theta) \times \{\text{Jacobi's standard elliptic integrals of the second kind}\}, \tag{19g}$$

where

$$\mathrm{sgn}(\theta) = \begin{cases} 1 & \text{if } \sin(\varphi - \theta) \leq 0, \\ -1 & \text{if } \sin(\varphi - \theta) > 0. \end{cases} \tag{19h}$$

There are $n+2$ unknowns in the foregoing elliptic integral formulation, namely either$(\theta_A, \theta_B, \theta_{C_1}, \theta_{C_2}, \ldots, \theta_{C_n})$ under displacement control or $(\theta_A, \theta_{C_1}, \theta_{C_2}, \ldots, \theta_{C_n}, \bar{U})$ under internal flow control of the stability of the pipe. Therefore, $n+2$ equations are required for solution, for instance equations (5d) and (11). Equation (5d) with the assistance of equations (15) and (18) can be expressed in elliptic integrals form as

$$\bar{y}_B = \bar{y}_{AC_1} + \bar{y}_{C_1C_2} + \bar{y}_{C_2C_3} + \cdots + \bar{y}_{C_{n-1}C_n} + \bar{y}_{C_nB} = 0, \tag{20a}$$

where for n being an even number,

$$\bar{y}_B = \frac{\sqrt{2}}{(b^2+c^2)^{3/4}}\left[\begin{array}{l} \eta(\Phi_A, k) - 2\eta(\Phi_{C_1}, k) + 2\eta(\Phi_{C_2}, k) \\ \qquad - \cdots - 2\eta(\Phi_{C_{n-1}}, k) + 2\eta(\Phi_{C_n}, k) - \eta(\Phi_B, k) \\ -\dfrac{2kc}{b}\left(\begin{array}{l} \cos\Phi_A - 2\cos\Phi_{C_1} + 2\cos\Phi_{C_2} \\ \quad - \cdots - 2\cos\Phi_{C_{n-1}} + 2\cos\Phi_{C_n} - \cos\Phi_B \end{array}\right) \end{array}\right] \tag{20b}$$

and when n is an odd number,

$$\bar{y}_B = \frac{\sqrt{2}}{(b^2+c^2)^{3/4}}\left[\begin{array}{l} -\eta(\Phi_A, k) + 2\eta(\Phi_{C_1}, k) - 2\eta(\Phi_{C_2}, k) \\ \qquad + \cdots - 2\eta(\Phi_{C_{n-1}}, k) + 2\eta(\Phi_{C_n}, k) - \eta(\Phi_B, k) \\ -\dfrac{2kc}{b}\left(\begin{array}{l} -\cos\Phi_A + 2\cos\Phi_{C_1} - 2\cos\Phi_{C_2} \\ \quad + \cdots - 2\cos\Phi_{C_{n-1}} + 2\cos\Phi_{C_n} - \cos\Phi_B \end{array}\right) \end{array}\right]. \tag{20c}$$

The system of nonlinear algebraic equations (11) and (20) is solved using the quasi-Newton method of minimization for the sake of global convergence (Press *et al.* 1992). The details of the iterative procedure are given in Chucheepsakul *et al.* (1999).

4. SHOOTING METHOD

In view of equations (2), (5), (7) and (8), another nondimensional form of the governing differential equations and the boundary conditions can be written as

$$\frac{\mathrm{d}\theta}{\mathrm{d}s^*} = \bar{s}_B[-\bar{K}\theta_A(\bar{x} + \Lambda\bar{y} - 1) - \bar{U}\bar{y}(\cos\theta_B - \Lambda\sin\theta_B)], \tag{21}$$

$$\frac{\mathrm{d}\bar{x}}{\mathrm{d}s^*} = \bar{s}_B\cos\theta, \quad \frac{\mathrm{d}\bar{y}}{\mathrm{d}s^*} = \bar{s}_B\sin\theta, \tag{22a,b}$$

$$\bar{x}(0) = 0, \quad \bar{y}(0) = 0, \quad \theta(0) = \theta_A, \quad \bar{x}(1) = 1, \quad \bar{y}(1) = 0, \quad \theta(1) = \theta_B. \tag{23a–f}$$

There are five unknowns in the above equations, namely either (θ, $\bar{x}$, $\bar{y}$, $\bar{s}_B$, θ_A) under displacement control or ($\bar{U}$, $\bar{x}$, $\bar{y}$, $\bar{s}_B$, θ_A) under internal flow control of the stability of the pipe. By employing the five end conditions of equations (23a–e), this boundary value problem under internal flow control could be solved by the following procedure.

Firstly, the shooting angle is prescribed by the initial values of equations (23d–f) and the guessed values of $\bar{s}_B$, $\bar{U}$ and θ_A. Secondly, the integration is carried out from $s^* = 1$ to 0 using the fifth-order Cash–Karp Runge–Kutta Fehlberg method (Press *et al.* 1992). Thirdly, the error norms are evaluated relative to the targets of equations (23a–c) and the following objective function Π is minimized using the downhill simplex method (Nelder & Mead 1965):

$$\underset{\bar{s}_B,\,\bar{U},\theta_A}{\text{Minimize}}\ \Pi = |\bar{x}(0)| + |\bar{y}(0)| + |\theta(0) - \theta_A|. \tag{24}$$

Finally, the foregoing steps are iterated until the allowable error is achieved.

5. STABILITY CRITERIA

The conventional approach for determining bifurcation criteria of the VAL elastica pipe is based on linear theory, which uses the small displacement assumption, $\mathrm{d}s \approx \mathrm{d}x, \theta \approx \mathrm{d}y/\mathrm{d}x$ and $\cos\theta \approx 1$, $\sin\theta \approx 0$. Thereby, equations (6) yield $C_1 = \rho_i A_i U^2$, $C_2 = C_3 = 0$, $R = 0$ and $\Lambda = \mp\mu$. By manipulating equations (2) and (4g), one obtains the boundary value problem of linear system,

$$y_{,xxxx} + \beta^2 y_{,xx} = 0 \tag{25a}$$

with the boundary conditions

$$y(0) = 0, \qquad y(L) = 0, \tag{25b,c}$$

$$y_{,xx}(0) = \hat{K}y_{,x}(0), \qquad y_{,xx}(L) = 0, \tag{25d,e}$$

where a subscript $(\ )_{,x} = \mathrm{d}(\ )/\mathrm{d}x$, $\beta^2 = \rho_i A_i U^2/EI$ and $\hat{K} = K/EI$.

Equation (25a) has the general solution

$$y = A_1\sin\beta x + A_2\cos\beta x + A_3 x + A_4, \tag{26}$$

in which A_1, A_2, A_3 and A_4 are constants depending on the boundary conditions.

Applying equation (26) to equations (25b–e) yields the characteristic equation

$$\begin{vmatrix} 0 & 1 & 0 & 1 \\ \sin\beta L & \cos\beta L & L & 1 \\ \hat{K}\beta & \beta^2 & \hat{K} & 0 \\ \beta^2 \sin\beta L & \beta^2 \cos\beta L & 0 & 0 \end{vmatrix} = 0. \tag{27}$$

Expansion of this determinant along with some manipulations yield

$$\tan u = \frac{\bar{K}u}{u^2 + \bar{K}}, \tag{28}$$

where $u = \beta L$, and u^2 is the dimensionless bifurcation velocity $\bar{U}_b$. For the case of simply supported VAL elastica pipes, $\bar{K} = 0$, thus equation (28) is simplified to $\tan u = 0$ or $\bar{U}_b = m^2\pi^2$, which is the well-known Euler buckling solution. For the case of fixed supported VAL elastica pipes, the limit of equation (28) when $\bar{K} \to \infty$ yields the characteristic equation $\tan u = u$.

On switching to the elastica theory, the same stability limits are derived from the condition

$$\bar{s}_B = \bar{s}_{AC_1} + \bar{s}_{C_1C_2} + \bar{s}_{C_2C_3} + \cdots + \bar{s}_{C_{n-1}C_n} + \bar{s}_{C_nB} = 1. \tag{29a}$$

Substituting equation (16) into equation (29a) yields the characteristic equations of stability limits as follows. For n being an even number,

$$\bar{s}_B = \frac{\sqrt{2}}{(b^2 + c^2)^{1/4}} \left[\begin{array}{l} \mathrm{F}(\Phi_A, k) - 2\mathrm{F}(\Phi_{C_1}, k) + 2\mathrm{F}(\Phi_{C_2}, k) \\ \qquad - \cdots - 2\mathrm{F}(\Phi_{C_{n-1}}, k) + 2\mathrm{F}(\Phi_{C_n}, k) - \mathrm{F}(\Phi_B, k) \end{array} \right] = 1 \tag{29b}$$

and for n being an odd number,

$$\bar{s}_B = \frac{\sqrt{2}}{(b^2 + c^2)^{1/4}} \left[\begin{array}{l} -\mathrm{F}(\Phi_A, k) + 2\mathrm{F}(\Phi_{C_1}, k) - 2\mathrm{F}(\Phi_{C_2}, k) \\ \qquad + \cdots - 2\mathrm{F}(\Phi_{C_{n-1}}, k) + 2\mathrm{F}(\Phi_{C_n}, k) - \mathrm{F}(\Phi_B, k) \end{array} \right] = 1. \tag{29c}$$

Equations (29) are easily examined by hand in the case of $\bar{K} = 0$ under the parameters simplified from equations (19) as follows:

$$\theta_i \to 0, \quad i = A, C_1, C_2, \ldots, C_n, B, \qquad a = -2\bar{U}_b, \qquad b = 0, \qquad c = 2\bar{U}_b, \tag{30a–c}$$

$$\varphi = 0, \qquad p = 2\bar{U}_b, \qquad \Phi_i = \frac{\pi}{2}, \qquad k = 0, \tag{30d–g}$$

$$\mathrm{F}(\Phi_i, k) = \mathrm{F}\left(\frac{\pi}{2}, 0\right) = \begin{cases} \dfrac{\pi}{2} & \text{if } \theta_i \to 0^+, \\ -\dfrac{\pi}{2} & \text{if } \theta_i \to 0^-, \end{cases} \qquad \frac{\sqrt{2}}{(b^2 + c^2)^{1/4}} = \frac{1}{\sqrt{\bar{U}_b}}. \tag{30h,i}$$

Substituting equations (30) into equations (29) yields the stability limit as

$$\bar{U}_b = (n + 1)^2\pi^2 = m^2\pi^2, \tag{31}$$

which is the Euler buckling solution as well. The numerical results of bifurcation velocity determined from equations (28) and (29) are found identical and are shown in Figure 5(b).

The numerical results of flow velocity–displacement curves shown in Figures (2) and 5(a) indicate that the bifurcation velocities $\bar{U}_b$ at the branching point are also the critical velocities. Nevertheless, when the support friction is taken into account, the critical

velocities are set apart from the bifurcation velocities as shown in Figure 4(a). In such a case, the critical velocities are determined using the dichotomous search method (Rao 1996).

6. RESULTS AND DISCUSSION

The elliptic integral method and the shooting method have been cross-checked for validating almost all of the postbuckling results presented in this study. An example to show validity of the solution is given in Table 1 in which numerical results are compared for the VAL elastica pipes with $\bar{K} = 0$ and $\mu = 0$. It is seen that the two methods yield almost identical results. However, the shooting method has advantage over the elliptic integral method in view of the unknown number, complexity of formulation, and independence of inflection points. To demonstrate the effects of arc-length variableness, of support friction, and of elastic rotational restraint on postbuckling behaviour of the VAL elastica pipe, the following three numerical examples with different boundary conditions are studied.

6.1. Simply Supported VAL Elastica Pipes

Figure 2 illustrates the relationship between the internal flow velocity $\bar{U}$ and the support rotations θ_A, θ_B of the constant-arc-length elastica pipe and the VAL elastica pipe. The equilibrium paths of the systems are along the vertical axis, the horizontal branching lines, and the ascendent and descendent branching curves. On the equilibrium paths overlying on the vertical axis, the three states of possible behaviour of the pipes may be explained as follows.

(a) *Stable state* (before a branching point). This state occurs when the pipes convey fluid with internal flow velocity less than the critical flow velocity $\bar{U}_{cr}$. In this state the VAL elastica pipe does not have both bending and sliding ($\theta_A = \theta_B = 0$) because no buckling has occurred. Consequently, there is no difference of behaviour between linear problems and elastica problems.

(b) *Critical state* (at a branching point). This state occurs when the pipes convey fluid with internal flow velocity equal to the critical flow velocity $\bar{U}_{cr}$. In this state the VAL elastica pipe still does not have both bending and sliding ($\theta_A = \theta_B = 0$) because of being in a transition state. This implies that the stability criteria of both linear problems and elastica problems are the same.

(c) *Unstable state* (over a branching point). This state occurs when the pipes convey fluid with internal flow velocity higher than the critical flow velocity $\bar{U}_{cr}$. All the points that belong to the flow velocity axis and are located above $\bar{U}_{cr}$ belong to this state. These equilibrium states are unstable and cannot be maintained if a disturbance, however small, is applied to the pipe. Practically, equilibrium paths will bifurcate along branching curves rather than going on this state.

On the equilibrium paths along the horizontal branching lines, and the ascendent and descendent branching curves, the three post-buckling states of the pipes may be explained as follows.

(i) *Stable post-buckling state* (along the ascendent branching curves) is the state that when $\bar{U}$ increases, the end rotations θ_A and θ_B will increase as well, and the elastica will be bent stably, namely a small disturbance does not affect to the equilibrium of the system. The constant-arc-length elastica pipe is on this state after buckling, as shown in Figure 2.

TABLE 1

Comparison of the post-buckling results for $\bar{K} = 0$ and $\mu = 0$

	θ_A(rad)		θ_B(rad)		$\frac{y_{\max}}{L}$		$\frac{s_B}{L}$		
Mode	EIM†	SM‡	EIM†	SM‡	EIM†	SM‡	EIM†	SM‡	$\bar{U}$
1	0·000000	0·000000	0·000000	0·000000	0·000000	0·000000	1·000000	1·000000	9·869604
	0·836105	0·836105	−0·836105	−0·836104	0·297307	0·297307	1·202689	1·202689	5
	1·570796	1·570799	−1·570796	−1·570795	0·834613	0·834614	2·188420	2·188422	0
2	0·000000	0·000000	0·000000	0·000000	0·000000	0·000000	1·000000	1·000000	39·478418
	−0·548471	−0·548472	−0·548471	−0·548471	0·091347	0·091347	1·079957	1·079957	30
	−0·836105	−0·836106	−0·836105	−0·836104	0·148653	0·148653	1·202689	1·202689	20
	−1·122793	−1·122796	−1·122793	−1·122792	0·221600	0·221600	1·418854	1·418856	10
	−1·570796	−1·570799	−1·570796	−1·570795	0·417309	0·417310	2·188420	2·188424	0
3	0·000000	0·000000	0·000000	0·000000	0·000000	0·000000	1·000000	1·000000	88·826440
	0·649662	0·649664	−0·649662	−0·649662	0·073533	0·073533	1·115105	1·115105	60
	0·897131	0·897134	−0·897131	−0·897130	0·108319	0·108319	1·239108	1·239108	40
	1·158453	1·158460	−1·158453	−1·158452	0·154968	0·154968	1·455472	1·455474	20
	1·320796	1·320806	−1·320796	−1·320794	0·192974	0·192975	1·662342	1·662348	10
	1·570796	1·570799	−1·570796	−1·570795	0·278206	0·278207	2·188420	2·188432	0
4	0·000000	0·000000	0·000000	0·000000	0·000000	0·000000	1·000000	1·000000	157·91367
	−0·548471	−0·548473	−0·548471	−0·548471	0·045673	0·047685	1·079957	1·079957	120
	−0·836105	−0·836108	−0·836105	−0·836104	0·074327	0·074348	1·202689	1·202690	80
	−1·122793	−1·122800	−1·122793	−1·122791	0·110800	0·110838	1·418854	1·418857	40
	−1·570796	−1·570799	−1·570796	−1·570794	0·208655	0·208665	2·188420	2·188441	0

† Elliptic integral method; ‡ Shooting Method.

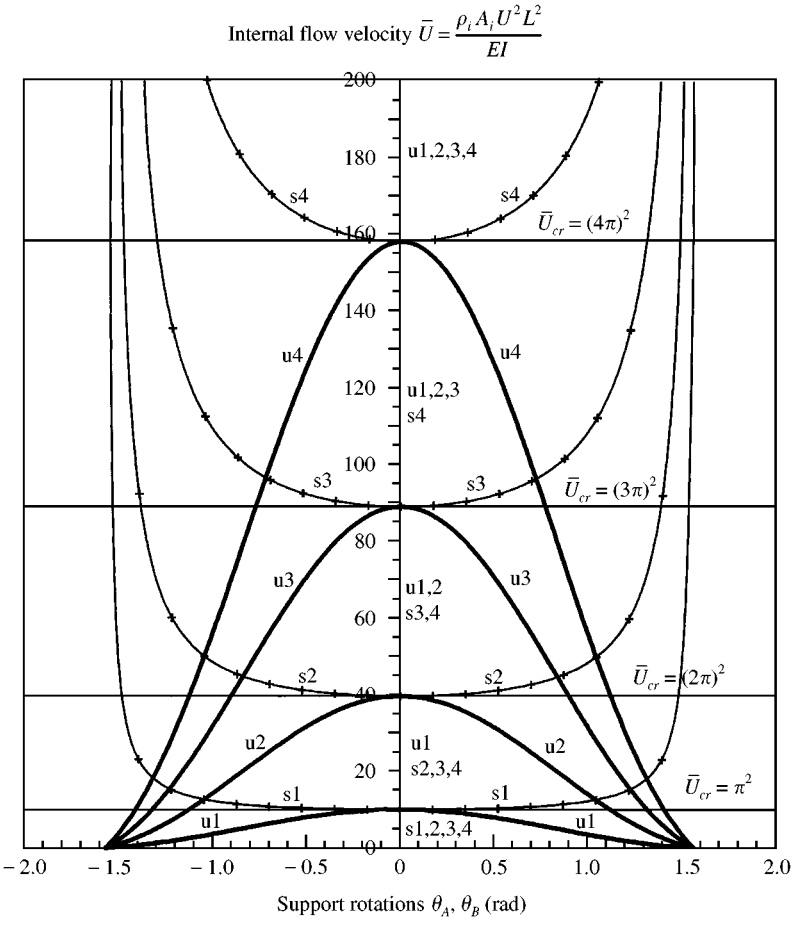

Figure 2. Relationship between internal flow velocity $\bar{U}$ and support rotations θ_A and θ_B for $\bar{K} = 0$ and $\mu = 0$. —+—, Elastica pipes with constant arc-length; ——, linear, small deflection; ——, elastica pipes with variable arc-length. The symbol 's' denotes stable state; and 'u', unstable state. The numbers 1,2,3,4 indicate instability mode numbers: 1,2,3,4, respectively.

(ii) *Neutral post-buckling state* (along the horizontal branching lines) is the state that the pipe may undergo small lateral deflections with no change of the critical flow velocity $\bar{U}_{cr}$. This state occurs only with the ideal pipe based on the linear analysis, as shown in Figure 2.

(iii) *Unstable post-buckling state* (along the descendent branching curves) is the state that when $\bar{U}$ decreases, the end rotations θ_A and θ_B increase instead of decreasing. This implies that after buckling, the pipe will be bent unstably, namely a small disturbance will initiate continuous pipe motion. The VAL elastica pipe is on this state after buckling, as shown in Figure 2.

The possible unstable equilibrium configurations of VAL elasticas transporting fluid with the steady flow velocity $\bar{U} = 6$ are displayed in Figure 3 for the 1st–4th buckling modes. It is found that for an equal $\bar{U}$, the elastica length $\bar{s}_B$ of higher-order modes is longer than that of lower-order modes. However, when the unstable equilibrium of all buckling modes of the VAL elastica pipe reaches the final state $\theta_A = \theta_B = \pi/2$, the arc-length of all the modes will become equal, and has the maximum value $\bar{s}_{B(\max)} = 2{\cdot}1884$ as shown in Table 1.

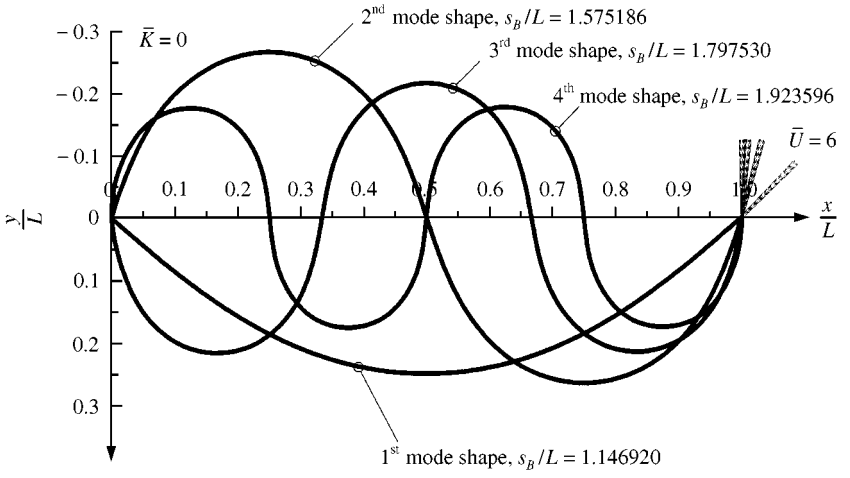

Figure 3. Unstable equilibrium configurations for $\bar{K} = 0$, $\mu = 0$, and $\bar{U} = 6$.

Chucheepsakul *et al.* (1995,1996,1997) were aware that this value is an invariant property of the single curvature bending of VAL elasticas under moment gradient, end moment, and point load.

6.2. Frictionally Supported VAL Elastica Pipes

The effect of friction at the support B is studied on the fundamental buckling mode by fixing $\bar{K} = 0$ and varying $\mu = 0$ to 1. Figure 4(a) shows the effect on flow velocity–displacement relationships in the case of $\mu = 0{\cdot}25$ and $0{\cdot}5$ for flow-loading condition (history of steady flow increase) and $\mu = -0{\cdot}25$ and $-0{\cdot}5$ for flow-unloading condition (history of steady flow decrease).

Under flow-loading conditions the equilibrium paths of the frictionally supported VAL elastica pipe are somewhat different from those of the simply supported VAL elastica pipe. Though their stable states are the same on the vertical axis, after bifurcation the branching

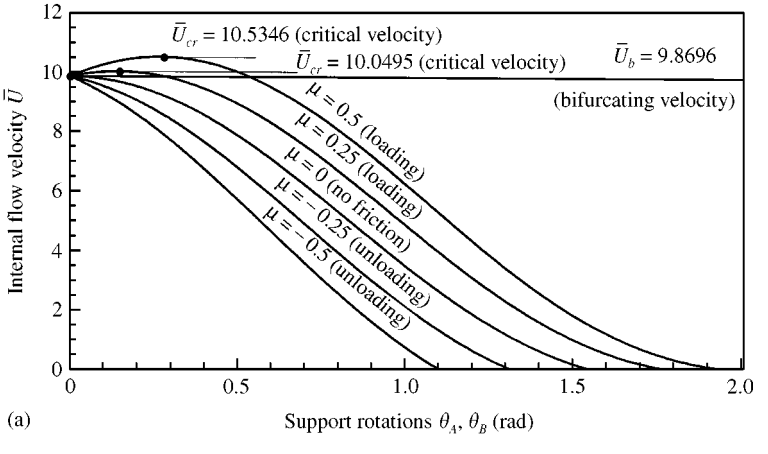

Figure 4. (a) Effect of friction coefficient μ on the relationship between internal flow velocity $\bar{U}$ and support rotations θ_A and θ_B.

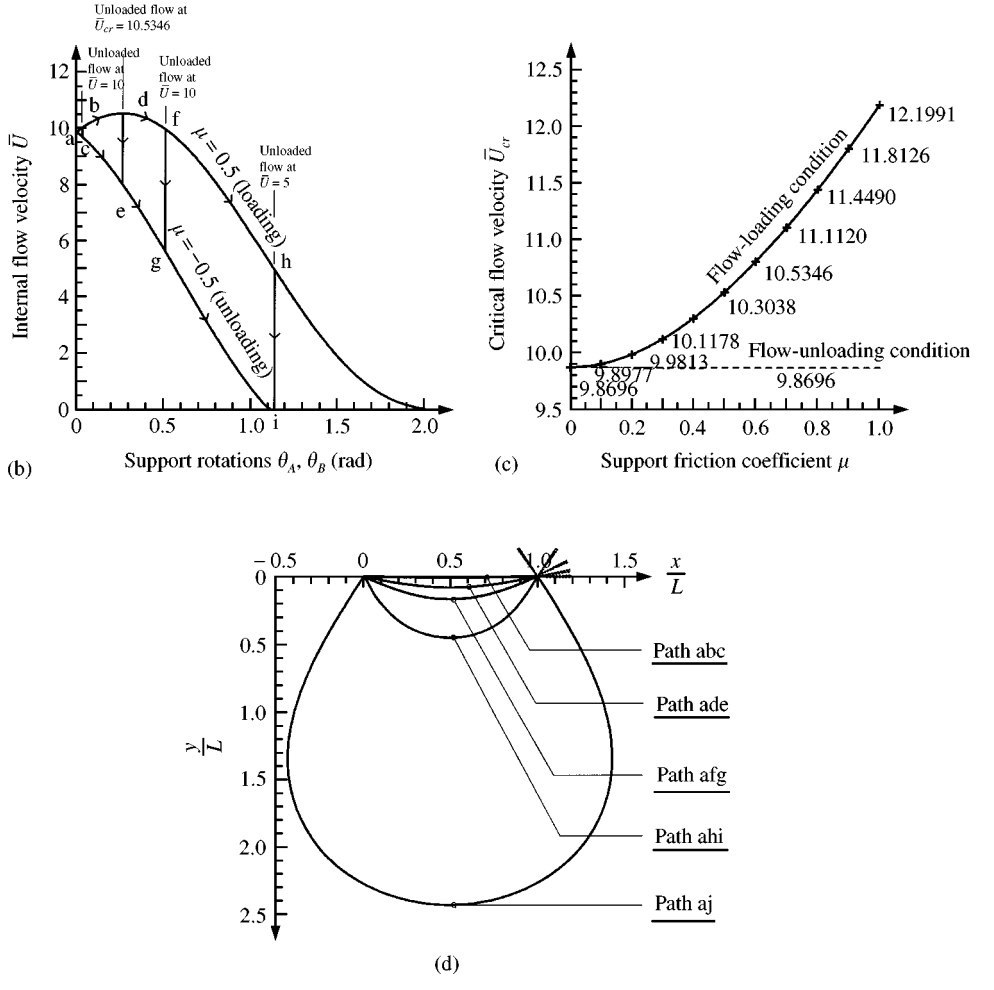

Figure 4. (continued) (b) Equilibrium path changes; (c) critical flow velocities $\bar{U}_{cr}$; (d) equilibrium configurations: path 'abc' is stable for $\bar{U} = 10$ (loading), and unstable for $\bar{U} = 10$–9·7259 (unloading); path 'ade' is critical for $\bar{U} = 10{\cdot}5346$ (loading), and unstable for $\bar{U} = 10{\cdot}5346$–8·0452 (unloading); path 'afg' is unstable for both $\bar{U} = 10$ (loading) and $\bar{U} = 10$–5·5703 (unloading); path 'ahi' is unstable for $\bar{U} = 5$ (loading), and no equilibrium for $\bar{U} = 5$ (unloading); path 'aj' is unstable for $\bar{U} = 0$ (loading), and no equilibrium for $\bar{U} = 0$ (unloading).

TABLE 2

Parameters of equilibrium path change corresponding to Figure 4(b)

		$\mu = 0{\cdot}5$		$\mu = -0{\cdot}5$		Stability status change
Path	s_B/L	θ_B(rad)	$\bar{U}$	θ_B(rad)	$\bar{U}$	Loading → Unloading
abc	1·0002	−0·0277	10	−0·0277	9·7259	Stable → unstable
ade	1·0174	−0·2618	10·5346	−0·2618	8·0452	Critical → unstable
afg	1·0696	−0·5136	10	−0·5136	5·5703	Unstable → unstable
ahi	1·4368	−1·1406	5	—	—	Unstable → no equilibrium exists

curves of the frictionally supported VAL pipe grow, corresponding to an increase of support rotations before reaching the critical point and their descent as shown in Figure 4(a). This means that, after buckling, the pipe will be in the stable post-buckling state, the critical post-buckling state, and the unstable post-buckling states, respectively. This behaviour could be explained as follows.

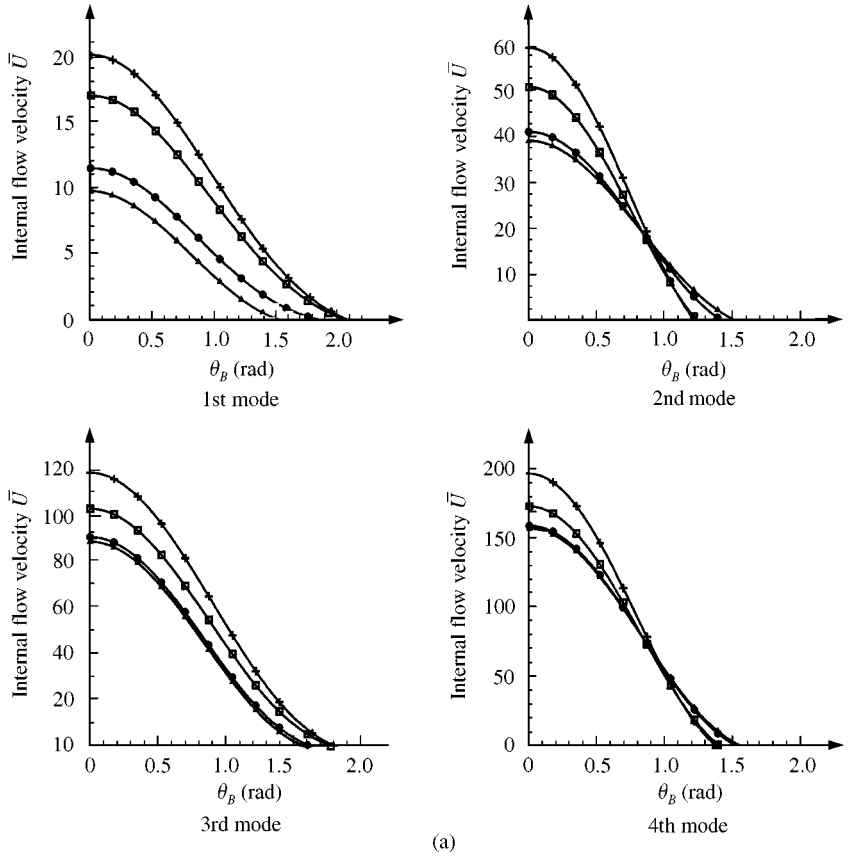

Range of $\bar{K}$		Characteristic equations
ⓐ	$\bar{K}=0$ $\bar{U}$	$\tan u = 0$
ⓐ to ⓑ	$0<\bar{K}<1000$ $\bar{U}$	$\tan u = \dfrac{\bar{K}u}{u^2+\bar{K}}$
over ⓑ	$\bar{K}\to\infty$ $\bar{U}$	$\tan u = u$

* Where $u=\sqrt{\bar{U}}=\sqrt{\dfrac{\rho_i A_i}{EI}}\,UL$

Figure 5. Effect of spring stiffness $\bar{K}$ on (a) the relationship between $\bar{U}$ and θ_B: —△—, $\bar{K}=0$; —●—, $\bar{K}=1$; —□—, $\bar{K}=10$; —+—, $\bar{K}=10\,000$; (b) critical flow velocity $\bar{U}_{cr}$.

Before branching, support friction has no effect on the bifurcation velocity, because it is still a nonworking force as long as the VAL pipes are motionless. Referring to equation (6d), $R(\theta_A = 0,\ \theta_B = 0) = 0$, and thus the friction force $\mu|R| = 0$. After branching, the friction force becomes a working force, to resist large displacements, and thus stabilizes the elastica. That yields an increase in the branching curves, which expresses the stable buckling state as explained in the previous topic. However, when the larger end-rotations are induced due to the higher internal flow velocity, it is seen that the branching curves tend to reach the peak value of $\bar{U}$, which is known as the maximum or critical value of $\bar{U}$ or $\bar{U}_{cr}$. There, the effect of support friction is no longer enough to stabilize the elastica; thus the system turns back to be dominated by the internal flow, and after that, it undergoes the unstable post-buckling state along the descending curves as shown in Figure 4(a).

Under flow-unloading conditions as shown in Figure 4(a), the equilibrium paths of the frictionally supported VAL elastica pipe are along the vertical axis, and the descendent branching curves as well as those of the simply supported VAL elastica pipes in the previous topic. The effect of support friction destabilizes the elastica owing to the opposite change of friction direction. Also, in Figure 4(a), it is seen that the locus of critical state is raised as the friction coefficient increases.

The direction of the support friction is nonconservative. If a flow-unloading condition happens due to any reduction of flow velocity such as partially closing the valve at inlet, the friction direction will be suddenly changed to the opposite direction. Consequently, the equilibrium path is abruptly altered, and then induced jumping between the equilibrium paths of flow-loading and flow-unloading conditions as shown in Figure 4(b). As a result, changes of stability status may occur as shown in Figure 4(b), paths abc, ade, afg, and ahi. The parameters of these paths are listed in Table 2, and the equilibrium configurations are shown in Figure 4(d). The effect of the support friction on critical velocity shown in Figure 4(c) is to increase the critical velocity under the flow-loading conditions, but have no influence under the flow-unloading conditions.

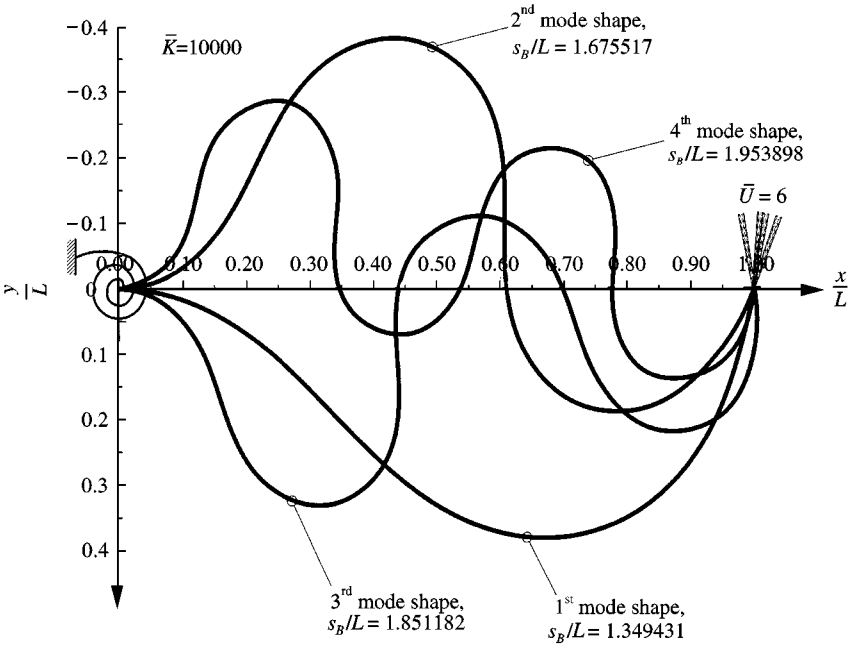

Figure 6. Unstable equilibrium configurations for $\bar{K} = 10\,000$, $\mu = 0$, and $\bar{U} = 6$.

6.3. Elastically Restrained VAL Elastica Pipes

The effect of elastic rotational restraint at the support A is studied in the 1st–4th buckling modes by fixing $\mu = 0$ and varying $\bar{K} = 0$–$10\,000$. Figure 5(a) shows the effect on the relationship between the flow velocity $\bar{U}$ and the support rotation θ_B for $\bar{K} = 0$, 1, 10, and 10 000. Figure 5(b) shows the effect on augmentation of the bifurcation and critical velocities in semi-log scale. It is observed that the critical velocities are almost constant for $\bar{K} \geq 1000$. For such a condition, support A may be considered as a fixed boundary condition.

The unstable equilibrium configurations of the VAL elasticas transporting fluid for $\bar{K} = 10\,000$, $\mu = 0$, and $\bar{U} = 6$ are displayed for the 1st–4th buckling modes in Figure 6. It is clearly seen that the elasticas are bent skew-forward in the odd buckling modes and skew-backward in the even buckling modes. As a thorough investigation towards these aspects, the authors detected the snap-throughs in the odd modes and the snap-backs in the even modes of instability whenever $\bar{K} > 0$. For example, in the case of $\bar{K} = 10\,000$ and $\mu = 0$, the complete flow velocity–displacement curves are shown and encircled with dashed line boxes on the ranges of snap-bending appearance in Figure 7.

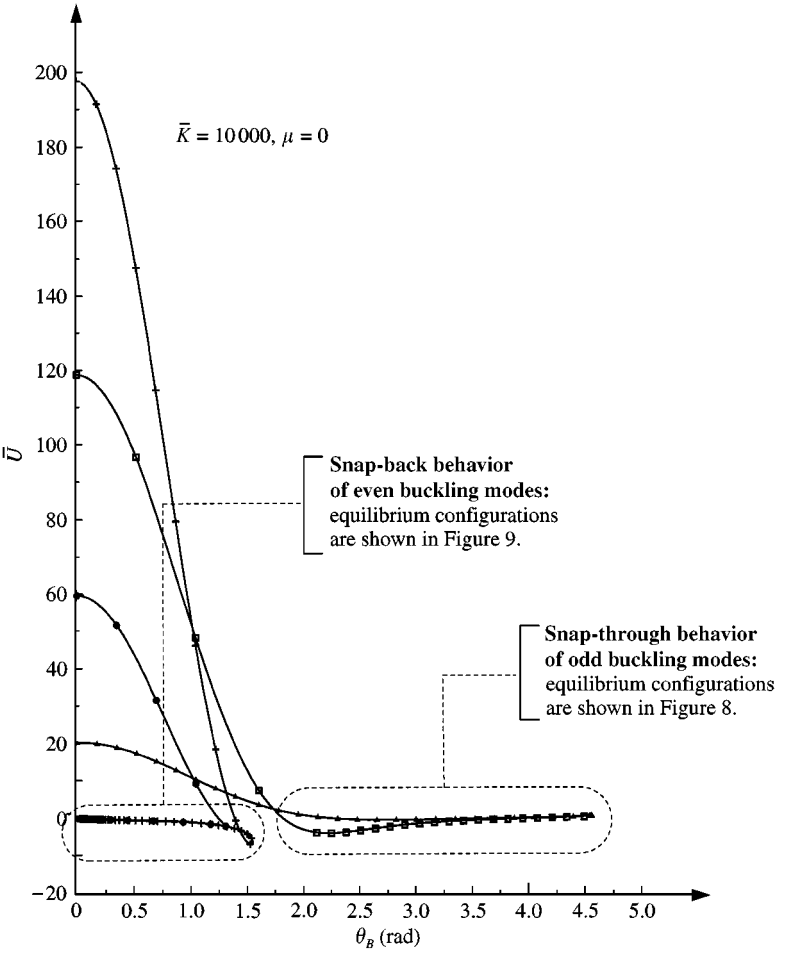

Figure 7. Relationship between $\bar{U}$ and θ_B for $\bar{K} = 10\,000$ and $\mu = 0$. —△—, First instability mode: —●—, second mode; —□—, third mode; —+—, fourth mode.

The snapping phenomena may be explained physically by comparing with the snap-bending behaviour of a shallow arch. As the arch is subjected to transversal load until a critical state, the snapping will occur suddenly to change the curvature of the arch from convex to concave. Likewise, after buckling, the unsymmetrical large deflection of the VAL elastica pipe enhances rolling the elasticas to the complex closed loops, as shown in the gradual formation process in Figures 8 and 9. Such behaviour brings about switching of every curvature of the elasticas either from concave to convex or from convex to concave.

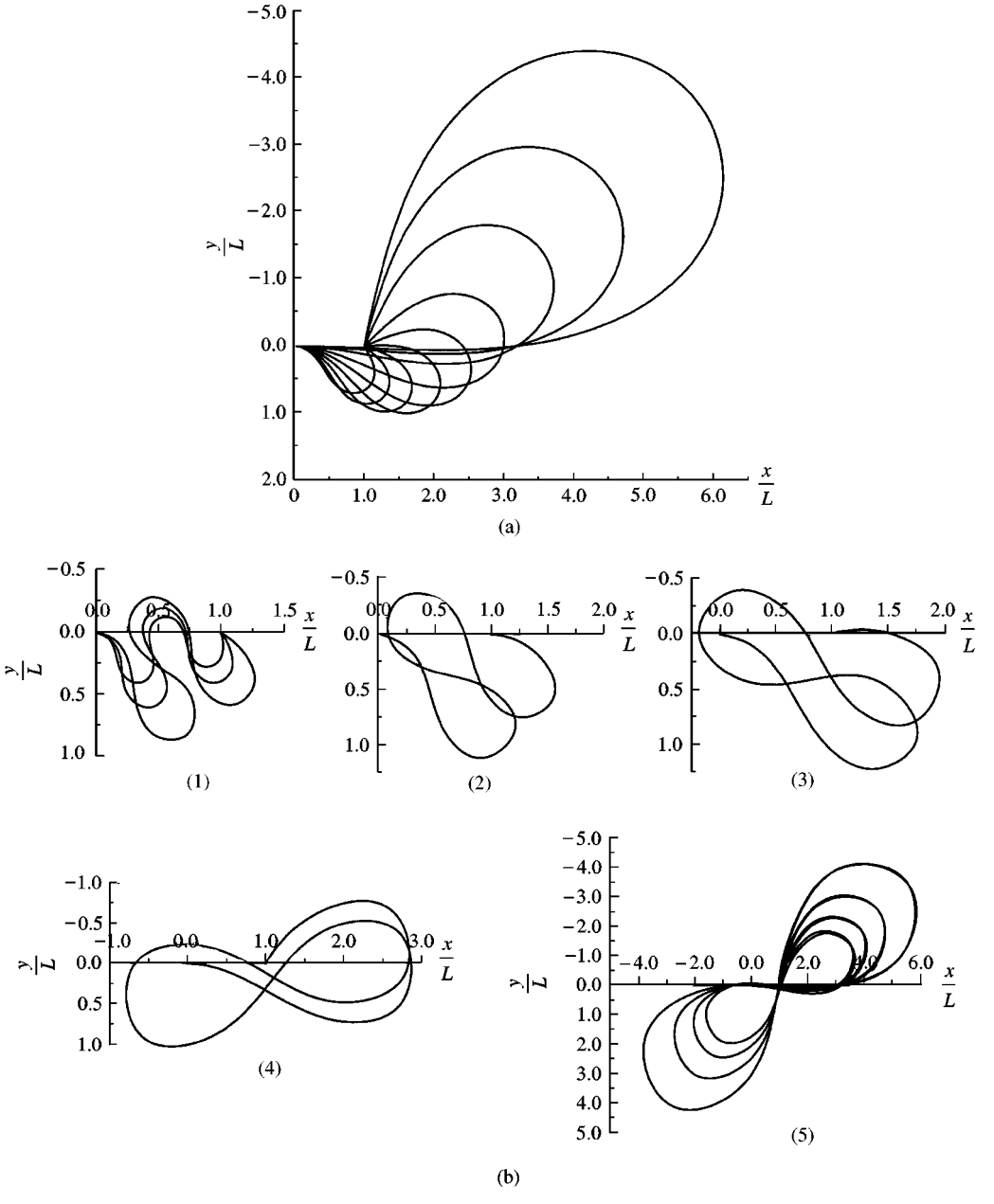

Figure 8. Loop formation of equilibrium configurations due to snap-throughs for $\bar{K} = 10\,000$ and $\mu = 0$: (a) the first instability mode; (b) the third instability mode.

With the same incentive as in the case of the shallow arch, the changes of all curvatures of the elastica pipe induce snapping phenomena as well.

The skew-forward bending of the elasticas in odd buckling modes induces snapping by the counterclockwise rotation of curvatures as shown in Figures 8, which is called snap-through. Conversely, the skew-backward bending of the elasticas in even buckling modes induces snapping by the clockwise rotation of curvatures as shown in Figures 9, which is

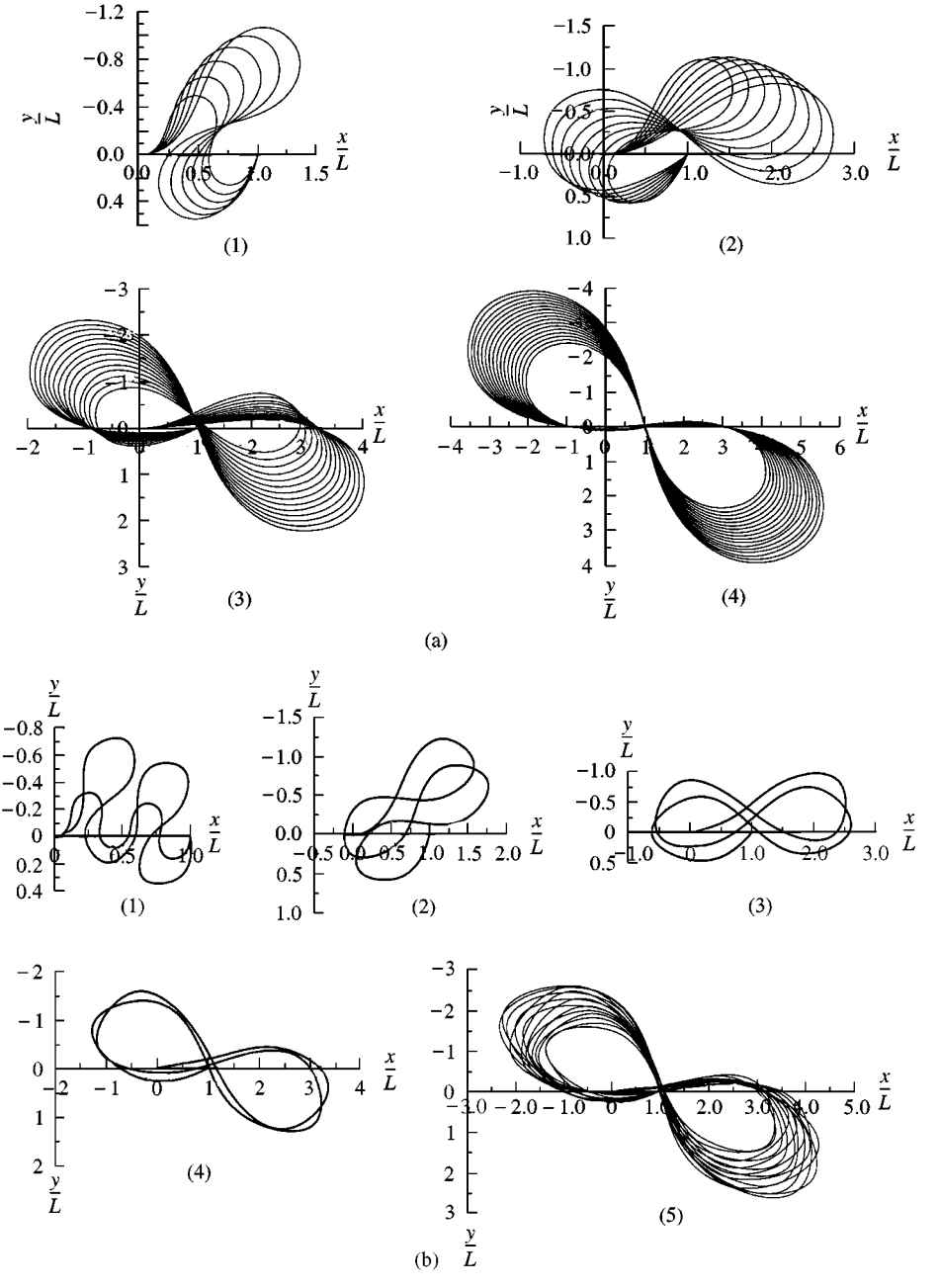

Figure 9. Loop formation of equilibrium configurations due to snap-backs for $\bar{K} = 10\,000$ and $\mu = 0$: (a) the second instability mode; (b) the fourth instability mode.

called snap-back. The complex closed-loop configurations of the elasticas are found akin to the loop soliton formation of a very long flexible elastic structure such as elastic metal band, rubber band or ribbon under chaotic motion, as shown by the experiments done by El Naschie (1990).

7. CONCLUDING REMARKS

The governing equations and post-buckling solutions for variable-arc-length elastica pipes transporting fluid with steady flow velocity are presented. The two approaches used to solve the problem, namely the elliptic integral method and shooting method, yield almost the same results. The branching limits obtained from the linear theory and the elastica theory are the same. After bifurcation, a simply supported elastica pipe with constant length buckles with stable bending, while the variable arc-length elastica pipe buckles with unstable bending.

Under flow-loading conditions, the support friction stabilizes the elasticas and increases the critical velocities. Under flow-unloading conditions, friction destabilizes the elasticas, but has no influence on branching states. The reduction of flow velocity may change the stability status of the elasticas due to a sudden change of friction direction. The effect of elastic rotational restraint is to stabilize the elasticas and to increase critical velocities. This effect leads to the unsymmetrical bending of at least two curvatures and eventually results in snap-bending behaviour.

ACKNOWLEDGEMENTS

The work reported in this paper is supported by the Thailand Research Fund (TRF) under Grant No. PHD/00132/2541. The authors would like to thank the anonymous reviewers for their valuable comments and suggestions.

References

Beck, M. 1952 Die knicklast des einseitig eingespannten, tangential gedrückten stabes. *Zeitschrift für angewandte Mathematik and Physik* **3,** 225–228.

Blevins, R. D. 1990 *Flow-Induced Vibration*, 2nd edition, pp. 384–399. New York: Van Nostrand Reinhold.

Byrd, P. F. & Friedman, M. D. 1971 *Handbook of Elliptic Integrals for Engineers and Scientists*, 2nd edition. Berlin: Springer-Verlag.

Chen, S. S. 1974 Flow-induced instability of an elastic tube. ASME paper No. 71-Vibr.-39.

Chucheepsakul, S., Buncharoen, S. & Huang, T. 1995 Elastica of simple variable arc-length beam subjected to an end moment. *ASCE Journal of Engineering Mechanics* **121,** 767–772.

Chucheepsakul, S., Theppitak, G. & Wang, C. M. 1996 Large deflection of simple variable-arc-length beam subjected to a point load. *Structural Engineering and Mechanics* **4,** 49–59.

Chucheepsakul, S., Theppitak, G. & Wang, C. M. 1997 Exact solutions of variable-arc-length elasticas under moment gradient. *Structural Engineering and Mechanics* **5,** 529–539.

Chucheepsakul, S., Wang, C. M., He, X. Q. & Monprapussorn T. 1999 Double curvature bending of variable-arc-length elasticas. *Journal of Applied Mechanics* **66,** 87–94.

El Naschie, M. S. 1990 *Stress, Stability and Chaos in Structural Engineering: an Energy Approach*, pp. 645–678. London: McGraw-Hill.

Elishakoff, I. & Lottati, I. 1988 Divergence and flutter of nonconservative system with intermediate support. *Computer Methods in Applied Mechanics and Engineering* **66,** 241–250.

Escobar, G. A. & Ting, A. E. 1986 A finite element computational procedure for the transient and stability behaviors of fluid conveying structures. In PVP-Vol. 101, pp. 61–72. New York: ASME.

Gregory, R. W. & Paidoussis, M. P. 1966 Unstable oscillation of tubular cantilevers conveying fluid. I. Theory. *Proceedings of the Royal Society* (*London*) A **293,** 512–527.

HOLMES, P. J. 1978 Pipes supported at both ends cannot flutter. *Journal of Applied Mechanics* **45,** 619–622.
HUANG, T. & CHUCHEEPSAKUL, S. 1985 Large displacement analysis of a marine riser. *ASME Journal of Energy Resources Technology* **107,** 54–59.
JENDRZEJCZYK, J. A. & CHEN, S. S. 1983 Experiments on tubes conveying fluid. Argonne National Laboratory Report ANL-83-18, Argonne, Illinois, U.S.A.
MOE, G. & CHUCHEEPSAKUL, S. 1988 The effect of internal flow on marine risers. *Proceedings of seventh International Offshore Mechanics and Arctic Engineering Symposium*, Vol. 1, pp. 375–382. New York: ASME.
NELDER, J. A. & MEAD, R. 1965 A simplex method for function minimization. *Computer Journal* **7,** 308–313.
PAÏDOUSSIS, M. P. 1998 *Fluid–Structure Interactions*: *Slender Structures and Axial Flow*, Vol. 1. New York: Academic Press.
PAÏDOUSSIS, M. P. & ISSID, N. T. 1974 Dynamic stability of pipes conveying fluid. *Journal of Sound and Vibration* **33,** 267–294.
PRESS, W. H., TEUKOLSKY, S. A., VETTERING, W. T. & FLANNERY, B. P. 1992 *Numerical Recipes in FORTRAN*, 2nd edition, pp. 372–381, 708–716. Cambridge: Cambridge University Press.
RAO, S. S. 1996 *Engineering Optimization*: *Theory and Practice*, 3rd edition, pp. 283–286. New York: Wiley-Interscience.
THOMPSON, J. M. T. 1982 *Instabilities and Catastrophes in Science and Engineering*, pp. 165–178. New York: Wiley-Interscience.
THOMPSON, J. M. T. & LUNN, T. S. 1981 Static elastica formulations of a pipe conveying fluid. *Journal of Sound and Vibration* **77,** 127–132.
YOSHIZAWA, M., NAO, H., HASEGAWA, E. & TSUJIOKA, Y. 1985 Buckling and post-buckling behaviour of a flexible pipe conveying fluid. *Bulletin of JSME* **28,** 1218–1225.

APPENDIX A: EQUILIBRIUM EQUATIONS

A.1. FORCES ACTING ON A FLUID ELEMENT

From Figure 1(b), the forces acting on a fluid element are

(i) the centrifugal force $= (\rho_i A_i \,\mathrm{d}s)a_n = \rho_i A_i U^2 \dfrac{\mathrm{d}s}{r} = \rho_i A_i U^2 \,\mathrm{d}\theta;$ (A.1)

(ii) the radial pressure force $= (p_i + \mathrm{d}p_i)A_i \sin(\mathrm{d}\theta/2) + p_i A_i \sin(\mathrm{d}\theta/2)$, but $\sin(\mathrm{d}\theta/2) \approx \mathrm{d}\theta/2$ and neglecting the higher-order term gives

$$\text{the radial pressure force} = \left(p_i \mathrm{d}\theta + \frac{\mathrm{d}p_i \,\mathrm{d}\theta}{2}\right)A_i = p_i A_i \,\mathrm{d}\theta; \tag{A.2}$$

(iii) the normal reaction between the fluid and pipe $F_n \mathrm{d}s$; from the Newton's second law ($\sum F_n =$ the centrifugal force),

$$F_n \,\mathrm{d}s - p_i A_i \,\mathrm{d}\theta = \rho_i A_i U^2 \,\mathrm{d}\theta,$$
$$F_n \,\mathrm{d}s = (\rho_i A_i U^2 + p_i A_i)\,\mathrm{d}\theta; \tag{A.3}$$

(iv) the tangential reaction between the fluid and pipe $F_t \,\mathrm{d}s$; because of U is constant ($a_t = 0$), therefore $\sum F_t = 0$,

$$F_t \,\mathrm{d}s - (p_i + \mathrm{d}p_i)A_i \cos\left(\frac{\mathrm{d}\theta}{2}\right) + p_i A_i \cos\left(\frac{\mathrm{d}\theta}{2}\right) - \tau \,\mathrm{d}s = 0,$$

but

$$\cos\left(\frac{\mathrm{d}\theta}{2}\right) \approx 1, \qquad F_t \,\mathrm{d}s - A_i \,\mathrm{d}p_i - \tau \,\mathrm{d}s = 0,$$

$$F_t \,\mathrm{d}s = A \,\mathrm{d}p + \tau \,\mathrm{d}s. \tag{A.4}$$

A.2. Forces Acting on a Pipe Element

From Figure 1(b), the forces acting on a pipe element are

(i) the normal reaction between the fluid and pipe $F_n\,\mathrm{d}s$;

$$F_n\,\mathrm{d}s - \left[(Q + \mathrm{d}Q)\cos\left(\frac{\mathrm{d}\theta}{2}\right) - Q\cos\left(\frac{\mathrm{d}\theta}{2}\right)\right] - \left[(T + \mathrm{d}T)\sin\left(\frac{\mathrm{d}\theta}{2}\right) + T\sin\left(\frac{\mathrm{d}\theta}{2}\right)\right] = 0,$$

$$F_n\,\mathrm{d}s = \mathrm{d}Q\cos\left(\frac{\mathrm{d}\theta}{2}\right) + (2T + \mathrm{d}T)\sin\left(\frac{\mathrm{d}\theta}{2}\right),$$

$$F_n\,\mathrm{d}s = \mathrm{d}Q + T\mathrm{d}\theta; \tag{A.5}$$

(ii) the tangential reaction between the fluid and the pipe $F_t\,\mathrm{d}s$;

$$F_t\,\mathrm{d}s + \left[(Q + \mathrm{d}Q)\sin\left(\frac{\mathrm{d}\theta}{2}\right) + Q\sin\left(\frac{\mathrm{d}\theta}{2}\right)\right] - \left[(T + \mathrm{d}T)\cos\left(\frac{\mathrm{d}\theta}{2}\right) - T\cos\left(\frac{\mathrm{d}\theta}{2}\right)\right] - \tau\mathrm{d}s = 0,$$

$$F_t\,\mathrm{d}s = \mathrm{d}T\cos\left(\frac{\mathrm{d}\theta}{2}\right) - (2Q + \mathrm{d}Q)\sin\left(\frac{\mathrm{d}\theta}{2}\right) + \tau\,\mathrm{d}s,$$

$$F_t\,\mathrm{d}s = \mathrm{d}T - Q\,\mathrm{d}\theta + \tau\,\mathrm{d}s. \tag{A.6}$$

A.3. Internal Force Equations

Combining equations (A.3) and (A.5) yields

$$\mathrm{d}Q + (T - \rho_i A_i U^2 - p_i A_i)\,\mathrm{d}\theta = 0. \tag{A.7}$$

Define now the combined tension (Moe & Chucheepsakul 1988)

$$N = T - p_i A_i - \rho_i A_i U^2. \tag{A.8}$$

Therefore, equation (A.7) becomes

$$\frac{\mathrm{d}Q}{\mathrm{d}\theta} + N = 0. \tag{A.9}$$

Likewise, by equality of equations (A.4) and (A.6), one obtains

$$\mathrm{d}T - Q\,\mathrm{d}\theta - A_i\,\mathrm{d}p_i = \mathrm{d}(T - p_i A_i - \rho_i A_i U^2) - Q\,\mathrm{d}\theta = 0,$$

$$\frac{\mathrm{d}N}{\mathrm{d}\theta} - Q = 0. \tag{A.10}$$

Taking a moment summation about the centre of curvature of the pipe element (point O),

$$-(M + \mathrm{d}M) + M - F_t\,\mathrm{d}s\left(r + \frac{\mathrm{d}_i}{2}\right) + (T + \mathrm{d}T)\,r - Tr + \tau\,\mathrm{d}s\,r = 0.$$

Since $r + \mathrm{d}_i/2 \approx r$, $F_t\,\mathrm{d}s = \mathrm{d}T - Q\,\mathrm{d}\theta + \tau\,\mathrm{d}s$ (equation (A.6)) and $r\,\mathrm{d}\theta = \mathrm{d}s$,

$$-\mathrm{d}M - (\mathrm{d}T - Q\,\mathrm{d}\theta)r + r\,\mathrm{d}T = -\mathrm{d}M + Q\,\mathrm{d}s = 0,$$

$$\frac{\mathrm{d}M}{\mathrm{d}s} - Q = 0. \tag{A.11}$$

Equations (A.9)–(A.11) are the general equilibrium differential equations of internal forces for 2-D inextensible analysis of the elastica pipe, neglecting its own weight.